 CMES, vol.82, no.1, pp.1-27, 2011

The Finite Point Method for Reaction–Diffusion Systems in Developmental Biology

Mehdi Tatari[1] **Maryam Kamranian**[2] **and Mehdi Dehghan**[2]

Abstract: In this paper, the finite point method (FPM) is presented for solving nonlinear reaction–diffusion systems which are often employed in mathematical modeling in developmental biology. In order to avoid directly solving a coupled nonlinear system, a predicator–corrector scheme is applied. The finite point method is a truly meshfree technique based on the combination of the moving least squares approximation on a cloud of points with the point collocation method to discretize the governing equations. The lack of dependence on a mesh or integration procedure is an important feature, which makes the FPM simple, efficient and applicable to solve nonlinear problems in complex domains. We present numerical solutions for two cases of interest, namely the well-studied Schnakenberg model and the Gierer–Meinhardt model, in various regions to demonstrate the effects of various domain geometries on the resulting biological patterns.

Keywords: Reaction–diffusion systems, Meshfree methods, Finite point method, MLS approximation, Developmental biology, Meshless techniques.

1 Introduction

1.1 The model investigated in the current work

A number of models used in biology, ecology and biochemistry comprise reaction of species in the presence of diffusion, hence reaction–diffusion systems arise. A particular case, driven by reaction and diffusion phenomenon, is characterized by the presence of space stable distributions of concentration species, commonly known as patterns [Garzón-Alvarado, Galeano, and Mantilla (2011)]. Alan M.

[1] Department of Mathematical Sciences Isfahan University of Technology, Isfahan, 84156-83111, Iran. E-mail address: mtatari@cc.iut.ac.ir (M. Tatari).

[2] Department of Applied Mathematics, Faculty of Mathematics and Computer Science, Amirkabir University of Technology, No. 424, Hafez Ave., 15914, Tehran, Iran.
E-mail addresses: m.kamranian@math.iut.ac.ir (M. Kamranian), mdehghan@aut.ac.ir; mdehghan.aut@gmail.com (M. Dehghan).

Turing [Turing (1952)], the British mathematician defined the conditions in which reactive phenomena at equilibrium cannot be stabilized by the presence of a diffusive term, forming spatial heterogeneous patterns known as instabilities driven by diffusion or Turing instabilities [Garzón-Alvarado, Galeano, and Mantilla (2011)].

Turing [Turing (1952); Madzvamuse (2000); Madzvamuse, Thomas, Maini, and Wathen (2002); Madzvamuse, Wathen, and Maini (2003, 2005); Madzvamuse and Maini (2007)] have proposed numerical simulations considering growing dominion conditions and particular geometries modifying distribution patterns. Their articles have a two species reaction–diffusion system in common as

$$\frac{\partial u}{\partial t} = \gamma f(u,v) + \nabla^2 u, \tag{1}$$

$$\frac{\partial v}{\partial t} = \gamma g(u,v) + d\nabla^2 v, \tag{2}$$

in which u and v are the two chemical concentrations, $d = \frac{d_v}{d_u}$ is the relationship between these species diffusion coefficients, while γ is a non–dimension coefficient associated with reactive processes f and g [Garzón-Alvarado, Galeano, and Mantilla (2011)].

In his seminal work, Turing found pattern formation in several physical and chemical processes. The present authors have been studying another biological situations like animal skin pattern formation [Frederik, Maini, Madzvamuse, Wathen, and Sekimura (2003); Rossi, Ristori, Rustici, Marchettini, and Tiezzi (2008); Madzvamuse, Wathen, and Maini (2003); Meinhardt (1982); Murray (1981); Sekimura, Madzvamuse, Wathen, and Maini (2000)], bone, tissue and tumor formation [Madzvamuse, Wathen, and Maini (2005); Ferreira, Martins, and Vilela (2002); García-Aznar, Kuiper, Gómez-Benito, Doblaré, and Richardson (2007); Chaplain, Ganesh, and Graham (2001)], animal population distribution [Baurmanna, Gross, and Feudel (2007); Yi, Wei, and Shi (2009)], in recent papers [Garzón-Alvarado, Galeano, and Mantilla (2011)]. Different numerical techniques for solution of the reaction–diffusion problem have thus been implemented, like finite differences [Murray (1981); Kondo and Asai (1995); Crampin, Gaffney, and Maini (1999); Barrio, Varea, Aragn, and Maini (1999)], finite elements [Madzvamuse, Thomas, Maini, and Wathen (2002); Madzvamuse, Wathen, and Maini (2003, 2005); Sekimura, Madzvamuse, Wathen, and Maini (2000); Chaplain, Ganesh, and Graham (2001)], spectral elements [Kassam and Trefethen (2003)] and finite volume spectral element method [Shakeri and Dehghan (2011)]. Many initial studies on Turing pattern formation have been devoted to work on fixed meshes. However, the growing nature of reaction–diffusion problems (in a biological context) has led to studies on growing meshes. For example, Madzvamuse [Madzvamuse, Wathen, and

Maini (2003)] has studied the incidence of mesh growth in diffusion pattern formation. In a seminal work, Madzvamuse [Madzvamuse, Wathen, and Maini (2003)] presented an algorithm for 2D diffusion–reaction problem solution using a continuously growing Eulerian dominion. For example, [Madzvamuse, Wathen, and Maini (2005)] introduced a mesh growing finite element technique for biological problems. In a recent paper the effect of advection on reaction–diffusion equations by using toroidal velocity fields has been studied by Garzón-Alvarado [Garzón-Alvarado, Galeano, and Mantilla (2011)].

1.2 The background of the proposed method

Here, we focus on a meshfree method for solving the reaction–diffusion system in complex domains. However we fix the domain problem but we believe that this method could be successfully implemented for reaction-diffusion problems in growing domains.

Meshfree methods have become quite popular for solving PDEs of physics and engineering. The motivation is to cut down modeling costs in the industrial applications by avoiding the labor intensive step of mesh generation. These methods are particularly attractive in problems with moving interfaces since no remeshing is necessary.

A family of meshfree methods is based on smooth particle hydrodynamic procedures [Monaghan (1992); Randles and Libersky (1996)]. A second class of meshfree methods derived from the generalized finite difference (GFD) techniques [Perrone and Kao (1975); Liszka and Orkisz (1975)]. Here the approximation around each point is typically defined in terms of Taylor series expansions and the discrete equations are found using the point collocation method. Among a third class of meshfree technique we find the so called diffuse element (DE) method [Nayroles, Touzot, and Villon (1992)], the element free Galerkin (EFG) method [Belytschko, Lu, and Gu (1994); Dolbow and Belytschko (1998)] and the reproducing kernel particle (RKP) method [Liu, Jun, Li, Adee, and Belytschko (1995); Liu, Chen, Jun, Chen, Belytschko, Pan, Uras, and Chang (1996)]. These three methods use the local interpolations for defining the approximate field around a point in terms of the values in adjacent points, whereas the discretized system of equations is typically obtained by integrating the Galerkin variational form over a suitable background grid.

The finite point method (FPM) proposed in [Onate, Idelsohn, Zienkiewicz, and Fisher (1995); Onate, Idelsohn, Zienkiewicz, and Taylor (1996a,b); Onate and Idelsohn (1998)] is a truly meshfree procedure. The approximation around each point is obtained using the standard moving least squares techniques similarly as in DE and EFG methods. The discrete system of equations is obtained by sampling the

governing differential equations at each point as in GFD methods. We refer the interested reader to [Atluri and Zhu (1998); Atluri (2005); Atluri and Shen (2002a,b); Dehghan and Mirzaei (2009); Mirzaei and Dehghan (2010)] for more research works on MLPG, [Tatari and Dehghan (2009); Shokri and Dehghan (2010); Dehghan and Shokri (2008)] on RBF and [Tatari, Kamranian, and Dehghan (2011); Boroomand, Najjar, and Onate (2009)] on finite point method. Also the reader can see [Dehghan and Ghesmati (2010); Kim and Liu (2006); Kim, Yoon, Liu, and Belytschko (2007); Kim, Liu, Yoon, Belytschko, and Lee (2007); Sladek, Sladek, and Atluri (2004); Sladek, Sladek, Hellmich, and Eberhardsteiner (2007); Sladek, Sladek, and J. Krivacek (2003); Sladek, Sladek, Tan, and Atluri (2008); Sladek, Sladek, and Zhang (2004); Zhu, Zhang, and Atluri (1998); Li and Liu (2004); Liu, Jun, and Zhang (1995); Liu, Li, and Belytschko (1997); Dehghan and Salehi (2011a,b)] for some applications of the meshless techniques.

In this work the finite point method is outlined for nonlinear reaction–diffusion systems. The reminder of this paper is organized as follows. In Section 2, the reaction–diffusion systems studied herein are briefly described. In Section 3, a time discretization and the finite point method are described for the proposed problem. The predicator–corrector scheme for solving the obtained nonlinear system is outlined in this section too. The numerical results for some problems involving the Schnakenberg and Gierer–Meinhardt models are investigated in Section 4. Finally a conclusion is drawn in Section 5.

2 The model equations

The numerical experiments in this paper are reaction–diffusion systems which have the general form

$$\frac{\partial \mathbf{u}}{\partial t} = \mathbf{D}\nabla^2\mathbf{u} + \gamma\mathbf{F}(\mathbf{u}) + \mathbf{P}(\mathbf{u}), \quad \text{in } \Omega \times [0,\infty), \tag{3}$$

where $\mathbf{u} = \begin{pmatrix} u \\ v \end{pmatrix}$, $\mathbf{F} = \begin{pmatrix} f(u,v) \\ g(u,v) \end{pmatrix}$, $\mathbf{P} = \begin{pmatrix} p(u,v) \\ q(u,v) \end{pmatrix}$, $\mathbf{D} = \begin{pmatrix} d_u & 0 \\ 0 & d_v \end{pmatrix}$, $\mathbf{x} = (x,y)$, where u and v are the two chemical concentrations under investigation, f, g, p and q are reaction kinetics, and $\mathbf{D}$ is the diffusion matrix (d_u and d_v are constant diffusion parameters). In a number of important applications the parameters γ, d_u and d_v are the most important and this is why they are explicitly included in (3).

Initial conditions are given by $\mathbf{u}(\mathbf{x},0) = \mathbf{u}_0(\mathbf{x})$ where $\mathbf{u}_0(\mathbf{x})$ is a prescribed nonnegative continuous bounded function. Boundary conditions can be of Dirichlet type or of (homogeneous) Neumann type which describe zero-flux of u (or v) out of the boundary. Initial conditions are defined as small random perturbations about the

uniform homogeneous steady state, if it exists (i.e., a state $u =$constant, $v =$ constant satisfying the boundary conditions and equation (3)) [Madzvamuse, Wathen, and Maini (2003)].

Below we consider three special cases where $\gamma \neq 0$ and $p(u,v) = q(u,v) = 0$.

2.1 Schnakenberg model

This is one of the simplest reaction diffusion models. It is derived from a series of hypothetical trimolecular autocatalistic reactions proposed by Schnakenberg [Schnakenberg (1979)]. In this model reaction kinetics are chosen in such a way that u activates the production of v while v inhibits the production of u.

In non-dimensional form the system is

$$\frac{\partial u}{\partial t} = \gamma(a - u + u^2 v) + \nabla^2 u, \tag{4}$$

$$\frac{\partial v}{\partial t} = \gamma(b - u^2 v) + d\nabla^2 v, \tag{5}$$

where $u(x,y,t)$ is the concentration of the activator, $v(x,y,t)$ is the concentration of the inhibitor, t is time and $\nabla^2 = \partial^2/\partial x^2 + \partial^2/\partial y^2$ is the two-dimensional Laplacian. a, b, d and γ are all non-dimensional positive parameters.

The biological interpretation of the reaction kinetics in Eqs. (4) and (5) is that u and v are produced at a constant rate γa and γb, respectively, while u is degraded linearly at rate γ. The nonlinear term $\gamma u^2 v$ implies the nonlinear activation of u and nonlinear consumption for v [Madzvamuse, Wathen, and Maini (2003)].

We remark that these characteristics are not peculiar to the Schnakenberg kinetics, also for other choices of the kinetic terms, including Gierer–Meinhardt kinetics.

2.2 Gierer–Meinhardt model

This is a model suggested by Gierer and Meinhardt [Gierer and Meinhardt (1972)]. The non–dimensional reaction diffusion system is given by

$$\frac{\partial u}{\partial t} = \gamma\left(a - bu + \frac{u^2}{v(1+ku^2)}\right) + \nabla^2 u, \tag{6}$$

$$\frac{\partial v}{\partial t} = \gamma(u^2 - v) + d\nabla^2 v, \tag{7}$$

in which a, b, d and γ are all non-dimensional positive parameters and k is a measure of the saturation concentration (see for example [Murray (1993)]).

The biological interpretation follows as above and the nonlinear term $\gamma u^2/\left(v(1+ku^2)\right)$ in Eq. (6) implies autocatalysis in u with saturation at high concentration values

of u and inhibition of u through the production of v. In Eq. (7), v is activated (produced) by u and degraded linearly.

2.3 Thomas model

This model is based on a specific substrate-inhibition reaction involving the substrates oxygen ($v(x,y,t)$) and uric acid ($u(x,y,t)$) which react in the presence of the enzyme uricase. The reaction kinetics, derived by fitting the kinetics to experimental data [Thomas and Kervenez (1975)], can be written in non–dimensional form as

$$\frac{\partial u}{\partial t} = \gamma\Big(a - u - h(u,v)\Big) + \nabla^2 u, \tag{8}$$

$$\frac{\partial v}{\partial t} = \gamma\Big(\alpha b - \alpha v - h(u,v)\Big) + d\nabla^2 v, \tag{9}$$

with $h(u,v) = \rho uv/(1+u+Ku^2)$. Here $a,\ b,\ d,\ \gamma,\ \alpha,\ \rho$ and K are positive parameters. The term $h(u,v)$ indicates the rate at which u and v are used up, in particular $h(u,v)$ exhibits what is known as substrate–inhibition, that is, for small u, $h(u,v)$ increases with u, while it decreases with large u.

2.4 Linear stability analysis

The parameter values in the reaction terms are those that give a constant uniform steady state in the absence of diffusion. The values of γ and the diffusion coefficient d are determined from the conditions that give rise to Turing instability. Turing instability or diffusion-driven instability occurs when a uniform steady state, linearly stable in the absence of diffusion, goes unstable in the presence of diffusion [Madzvamuse, Wathen, and Maini (2003)]. The process of determining these parameter values is known as linear stability analysis.

We recall from [Murray (1993)] (Section 2.3) some results on the conditions under which a diffusion-driven instability of a uniform steady state of the systems (4)-(9) occurs. The necessary condition is that the inequalities

$$f_u + g_v < 0,$$

$$f_u g_v - f_v g_u > 0,$$

$$d f_u + g_v > 0,$$

$$(d f_u + g_v)^2 - 4d(f_u g_v - f_v g_u) > 0,$$

are satisfied at $(u,v) = (u_s, v_s)$ in which $f_u,\ f_v,\ g_u$ and g_v indicate the derivatives of the reaction functions regarding concentration variables (for example $f_u = \frac{\partial f}{\partial u}$).

These inequalities define a parameter space, known as the Turing space, wherein the uniform steady state is unstable to random small perturbations.

From the stability analysis [Murray (1993)] in the unit square with zero flux boundary conditions, the parameter values d and γ corresponding to the spatial mode $\cos(m\pi x)\cos(n\pi y)$ denoted by (m,n), are shown in Tab. 1, for some fixed parameter values:

- Schnakenberg model: $a = 0.1,\ b = 0.9$,
- Gierer–Meinhardt model: $a = 0.1,\ b = 1.0,\ k = 0.5$,
- Thomas model: $a = 150,\ b = 100,\ K = 0.05,\ \alpha = 1.5,\ \rho = 13$.

This table has been extracted from [Madzvamuse, Wathen, and Maini (2003)].

3 The numerical implementation

For illustrative purposes, let us consider the standard two species reaction–diffusion system as

$$\frac{\partial u}{\partial t} = \gamma f(u,v) + \nabla^2 u, \tag{10}$$

$$\frac{\partial v}{\partial t} = \gamma g(u,v) + d\nabla^2 v, \tag{11}$$

in $\Omega \times [0,\infty)$, $\Omega \subset \mathbb{R}^2$ with the initial conditions

$$u(\mathbf{x},0) = u_0(\mathbf{x}), \quad v(\mathbf{x},0) = v_0(\mathbf{x}), \quad \mathbf{x} = (x,y) \in \Omega,$$

and the homogenous Neumann boundary conditions

$$\frac{\partial u}{\partial n}(\mathbf{x},t) = 0, \quad \frac{\partial v}{\partial n}(\mathbf{x},t) = 0, \quad \mathbf{x} \in \partial\Omega.$$

3.1 The time discretization

To deal with the time derivative, a Crank–Nicolson discretization is employed. The main reason for choosing this method is the high order of convergence. In this technique, a time step, Δt is selected and then the differential Eqs. (10) and (11) at the time $t + 1/2\Delta t$ are evaluated. The time derivative is approximated with a centered finite difference. For the rest terms, the average of times t and $t + \Delta t$ is

Table 1: Values for d and γ under which a particular mode is isolated on a unit square domain for the Gierer–Meinhardt, Thomas and Schnakenberg models

Mode (m,n)	Gierer–Meinhardt		Thomas		Schnakenberg	
	d	γ	d	γ	d	γ
(1,0)	520.1573	67	427.0152	44	10	29
(1,1)	105.1573	168.8	39.0152	79	11.5776	70.6
(2,0)	84.1573	238.26	54.0152	122	10	114
(2,1)	77.6473	411.42	29.0152	170	9.1676	176.72
(2,2)	75.1573	483.43	30.9152	252	8.6676	230.82
(3,0)	70.8473	619.45	36.0152	269	8.6176	265.22
(3,1)	72.1573	756.23	27.5152	320	8.6676	329.20
(3,2)	73.1573	901.38	28.4152	402	8.8676	379.21
(3,3)	70.5573	1266.99	28.5152	553	8.6076	535.09
(4,0)	71.1573	1033.51	31.5152	473	8.6676	435.99
(4,1)	70.3573	1164.86	27.0252	506	8.5876	492.28
(4,2)	71.1573	1519.87	27.0252	596	8.7176	625.35
(4,3)	71.1573	1580.66	27.0252	745	8.6676	666.82
(4,4)	73.1473	2167	27.0252	953	8.6076	909.66

considered. Therefore the Eqs. (10) and (11) can be written as:

$$u^{(k+1)} - \beta\left(\gamma f(u^{(k+1)}, v^{(k+1)}) + \nabla^2 u^{(k+1)}\right) = u^{(k)} + \beta\left(\gamma f(u^{(k)}, v^{(k)}) + \nabla^2 u^{(k)}\right), \tag{12}$$

$$v^{(k+1)} - \beta\left(\gamma g(u^{(k+1)}, v^{(k+1)}) + d\nabla^2 v^{(k+1)}\right) = v^{(k)} + \beta\left(\gamma g(u^{(k)}, v^{(k)}) + d\nabla^2 v^{(k)}\right), \tag{13}$$

in which $u^{(k)}(\mathbf{x}) = u(\mathbf{x}, k\Delta t)$, $v^{(k)}(\mathbf{x}) = v(\mathbf{x}, k\Delta t)$ and $\beta = \Delta t/2$.

3.2 The Finite Point Method

The finite point method (FPM) employs a weighted least squares technique to construct the meshfree approximation function and a point collocation procedure in order to discretize the governing partial differential equations.
To approximate $u^{(k)}(\mathbf{x}) = u(\mathbf{x}, k\Delta t)$ in the problem domain Ω, over a number of randomly located nodes $\{\mathbf{x}_i\}$, $i = 1, 2, ..., n$, the moving least squares approximation $u_h^{(k)}(\mathbf{x})$ of $u^{(k)}(\mathbf{x})$, $\forall \mathbf{x} \in \bar{\Omega}$, can be defined by

$$u_h^{(k)}(\mathbf{x}) = \mathbf{p}^T(\mathbf{x})\mathbf{a}^{(k)}(\mathbf{x}), \qquad \forall \mathbf{x} \in \bar{\Omega}, \tag{14}$$

where $\mathbf{p}^T(\mathbf{x}) = [p_1(\mathbf{x}), p_2(\mathbf{x}), ..., p_m(\mathbf{x})]$ is a complete monomial basis of order m and $\mathbf{a}^{(k)}(\mathbf{x})$ is a vector containing coefficients $a_j^{(k)}(\mathbf{x})$, $j = 1, 2, ..., m$ which are functions of the space coordinates $\mathbf{x}$. For example for a 2-D problem,
$\mathbf{p}^T(\mathbf{x}) = [1, x, y]$, linear basis, $m = 3$
$\mathbf{p}^T(\mathbf{x}) = [1, x, y, x^2, xy, y^2]$, quadratic basis, $m = 6$.
The unknown parameters $a_j^{(k)}(\mathbf{x})$ are determined at any point $\mathbf{x}$, by minimizing a functional $\mathscr{J}(\mathbf{x})$ defined by

$$\mathscr{J}(\mathbf{x}) = \sum_{i=1}^{n} w(\mathbf{x} - \mathbf{x}_i)\left(u_h^{(k)}(\mathbf{x}_i) - u_i^{(k)}\right)^2 = \sum_{i=1}^{n} w(\mathbf{x} - \mathbf{x}_i)\left(\mathbf{p}^T(\mathbf{x}_i)\mathbf{a}^{(k)}(\mathbf{x}) - u_i^{(k)}\right)^2, \tag{15}$$

where $w(\mathbf{x} - \mathbf{x}_i)$ is the weight function with compact support associated with node i, n is the number of nodes in $\bar{\Omega}$ for which the weight function $w(\mathbf{x} - \mathbf{x}_i) > 0$ and the parameters $u_i^{(k)}$ are specified. Eq. (15) can be written as

$$\mathscr{J}(\mathbf{x}) = [\mathbf{P}.\mathbf{a}^{(k)}(\mathbf{x}) - \mathbf{u}^{(k)}]^T.\mathbf{W}.[\mathbf{P}.\mathbf{a}^{(k)}(\mathbf{x}) - \mathbf{u}^{(k)}], \tag{16}$$

where

$$\mathbf{P}=\begin{bmatrix}\mathbf{p}^T(\mathbf{x}_1)\\ \mathbf{p}^T(\mathbf{x}_2)\\ \vdots\\ \mathbf{p}^T(\mathbf{x}_n)\end{bmatrix}_{n\times m},\mathbf{W}=\begin{bmatrix}w(\mathbf{x}-\mathbf{x}_1) & \cdots & \mathbf{0}\\ \cdots & \ddots & \cdots\\ \mathbf{0} & \cdots & w(\mathbf{x}-\mathbf{x}_n)\end{bmatrix}_{n\times n}.$$

The standard minimization of (16) with respect to $\mathbf{a}^{(k)}(\mathbf{x})$ can be obtained by setting the derivative of $\mathscr{J}$ with respect to $\mathbf{a}^{(k)}(\mathbf{x})$ equal to zero. The following linear system results:

$$\mathbf{A}(\mathbf{x})\mathbf{a}^{(k)}(\mathbf{x})=\mathbf{D}(\mathbf{x})\mathbf{u}^{(k)}, \tag{17}$$

where matrices $\mathbf{A}(\mathbf{x})$ and $\mathbf{D}(\mathbf{x})$ are defined by

$$\mathbf{A}(\mathbf{x})=\mathbf{P}^T\mathbf{W}\mathbf{P}=\sum_{i=1}^{n}w(\mathbf{x}-\mathbf{x}_i)\mathbf{p}(\mathbf{x}_i)\mathbf{p}^T(\mathbf{x}_i), \tag{18}$$

$$\mathbf{D}(\mathbf{x})=\mathbf{P}^T\mathbf{W}=[w(\mathbf{x}-\mathbf{x}_1)\mathbf{p}(\mathbf{x}_1),w(\mathbf{x}-\mathbf{x}_2)\mathbf{p}(\mathbf{x}_2),...,w(\mathbf{x}-\mathbf{x}_n)\mathbf{p}(\mathbf{x}_n)]. \tag{19}$$

Solving for $\mathbf{a}^{(k)}(\mathbf{x})$ from Eq. (17) and substituting it into Eq. (14), the MLS approximation can be defined as

$$u_h^{(k)}(\mathbf{x})=\sum_{i=1}^{n}\phi_i(\mathbf{x})u_i^{(k)}=\Phi^T(\mathbf{x})\mathbf{u}^{(k)},\quad \mathbf{x}\in\bar{\Omega}, \tag{20}$$

where

$$\Phi^T(\mathbf{x})=\mathbf{p}^T(\mathbf{x})\mathbf{A}^{-1}(\mathbf{x})\mathbf{D}(\mathbf{x}), \tag{21}$$

or for the shape function $\phi_i(\mathbf{x})$ associated with node i at a point $\mathbf{x}$ we have

$$\phi_i(\mathbf{x})=\sum_{j=1}^{m}p_j(\mathbf{x})\left(\mathbf{A}^{-1}(\mathbf{x})\mathbf{D}(\mathbf{x})\right)_{ji}. \tag{22}$$

The matrix $\mathbf{A}(\mathbf{x})$ is often called the moment matrix, it is of size $m\times m$. This matrix must be inverted whenever the MLS shape functions are to be evaluated. It can be seen that this is the case if and only if the rank of $\mathbf{P}$ equals m. A necessary condition for a well–defined MLS approximation is that at least m weight functions are non–zero (i.e. $n\geq m$) for each sample point $\mathbf{x}\in\Omega$ [Zuppa (2003)].

A similar approximation can be written for $v^{(k)}(\mathbf{x}) = v(\mathbf{x}, k\Delta t)$ as

$$v_h^{(k)}(\mathbf{x}) = \sum_{i=1}^{n} \phi_i(\mathbf{x}) v_i^{(k)} = \Phi^T(\mathbf{x})\mathbf{v}^{(k)}, \quad \mathbf{x} \in \bar{\Omega}. \tag{23}$$

The smoothness of the shape functions $\phi_i(\mathbf{x})$ is determined by that of the basis functions and of the weight functions. If $w(\mathbf{x}-\mathbf{x}_i) \in C^k(\Omega)$ and $p_j(\mathbf{x}) \in C^l(\Omega)$, $i = 1,2,...,n$, $j = 1,2,...,m$, then $\phi_i(\mathbf{x}) \in C^{min(k,l)}(\Omega)$. The partial derivatives of $\phi_i(\mathbf{x})$ are obtained as

$$\phi_{i,k}(\mathbf{x}) = \sum_{j=1}^{m} \left(p_{j,k}(\mathbf{A}^{-1}\mathbf{D})_{ji} + p_j(\mathbf{A}^{-1}\mathbf{D}_{,k} + \mathbf{A}_{,k}^{-1}\mathbf{D})_{ji} \right), \tag{24}$$

and

$$\begin{aligned} \phi_{i,kl}(\mathbf{x}) = \sum_{j=1}^{m} \Big(& p_{j,kl}(\mathbf{A}^{-1}\mathbf{D})_{ji} + p_j(\mathbf{A}_{,l}^{-1}\mathbf{D}_{,k} + \mathbf{A}^{-1}\mathbf{D}_{,kl} + \mathbf{A}_{,kl}^{-1}\mathbf{D} + \mathbf{A}_{,k}^{-1}\mathbf{D}_{,l})_{ji} \\ & + p_{j,k}(\mathbf{A}^{-1}\mathbf{D}_{,l} + \mathbf{A}_{,l}^{-1}\mathbf{D})_{ji} + p_{j,l}(\mathbf{A}^{-1}\mathbf{D}_{,k} + \mathbf{A}_{,k}^{-1}\mathbf{D})_{ji} \Big), \end{aligned} \tag{25}$$

where, $(\,)_{,k}$ and $(\,)_{,kl}$ denote $\partial(\,)/\partial x_k$ and $\partial^2(\,)/\partial x_{kl}$, respectively. Also $\mathbf{A}_{,k}^{-1} = (\mathbf{A}^{-1})_{,k}$ represents the derivative of the inverse of $\mathbf{A}$ with respect to x_k, which is given by

$$\mathbf{A}_{,k}^{-1} = -\mathbf{A}^{-1}\mathbf{A}_{,k}\mathbf{A}^{-1}, \tag{26}$$

where

$$\mathbf{A}_{,k}(\mathbf{x}) = \sum_{i=1}^{n} w_{,k}(\mathbf{x}-\mathbf{x}_i)\mathbf{p}(\mathbf{x}_i)\mathbf{p}^T(\mathbf{x}_i). \tag{27}$$

So the first order and the second order partial derivatives of $u_h^{(k)}(\mathbf{x})$ are obtained by

$$\frac{\partial}{\partial x_k} u_h^{(k)}(\mathbf{x}) = \sum_{i=1}^{n} \phi_{i,k}(\mathbf{x}) u_i^{(k)}, \quad \mathbf{x} \in \bar{\Omega}, \tag{28}$$

and

$$\frac{\partial^2}{\partial x_k \partial x_l} u_h^{(k)}(\mathbf{x}) = \sum_{i=1}^{n} \phi_{i,kl}(\mathbf{x}) u_i^{(k)}, \quad \mathbf{x} \in \bar{\Omega}, \tag{29}$$

respectively.

When the meshfree approximation functions are constructed, the finite point method uses a point collocation technique to discretize the governing equations. The point collocation approach gives rise to a system of equations, the solution of which provides the nodal parameters at the nodes. Once the nodal parameters are computed, the unknown solution at each node can be computed from Eqs. (20) and (23).

To express the details of the method, we focus on the Schnakenberg model

$$\frac{\partial u}{\partial t} = \gamma\Big(a - u + u^2 v\Big) + \nabla^2 u, \tag{30}$$

$$\frac{\partial v}{\partial t} = \gamma\Big(b - u^2 v\Big) + d\nabla^2 v. \tag{31}$$

So Eqs. (12) and (13) can be simplified to

$$u^{(k+1)} - \beta\left(\nabla^2 u^{(k+1)} + \gamma\Big(-u^{(k+1)} + (u^{(k+1)})^2 v^{(k+1)}\Big)\right) =$$

$$u^{(k)} + \beta\left(\nabla^2 u^{(k)} + \gamma\Big(-u^{(k)} + (u^{(k)})^2 v^{(k)}\Big)\right) + 2\beta\gamma a, \tag{32}$$

$$v^{(k+1)} - \beta\Big(d\nabla^2 v^{(k+1)} - \gamma(u^{(k+1)})^2 v^{(k+1)}\Big) =$$

$$v^{(k)} + \beta\Big(d\nabla^2 v^{(k)} - \gamma(u^{(k)})^2 v^{(k)}\Big) + 2\beta\gamma b, \tag{33}$$

in which $\beta = \Delta t/2$. To apply the scheme we consider n nodal points $\{\mathbf{x}_j\}_{j=1}^n$ in the domain of the problem and on its boundary as MLS nodal points. Substituting (20) and (23) into Eqs. (32) and (33) and using the collocation at each interior node $\mathbf{x}_j$ (i.e. $\mathbf{x}_j \in \text{int}\,(\Omega)$), result in,

$$u_j^{(k+1)} - \beta\left(\nabla^2 u_j^{(k+1)} + \gamma\Big(-u_j^{(k+1)} + (u_j^{(k+1)})^2 v_j^{(k+1)}\Big)\right) =$$

$$u_j^{(k)} + \beta\left(\nabla^2 u_j^{(k)} + \gamma\Big(-u_j^{(k)} + (u_j^{(k)})^2 v_j^{(k)}\Big)\right) + 2\beta\gamma a, \qquad \mathbf{x}_j \in \text{int}\,(\Omega), \tag{34}$$

$$v_j^{(k+1)} - \beta\Big(d\nabla^2 v_j^{(k+1)} - \gamma(u_j^{(k+1)})^2 v_j^{(k+1)}\Big) =$$

$$v_j^{(k)} + \beta\Big(d\nabla^2 v_j^{(k)} - \gamma(u_j^{(k)})^2 v_j^{(k)}\Big) + 2\beta\gamma b, \qquad \mathbf{x}_j \in \text{int}\,(\Omega), \tag{35}$$

where

$$u_j^{(k)} = u(\mathbf{x}_j, t^{(k)}), \quad v_j^{(k)} = v(\mathbf{x}_j, t^{(k)}),$$

$$\nabla^2 u_j^{(k)} = \sum_{i=1}^{n}\left(\frac{\partial^2 \phi_i}{\partial x^2}(\mathbf{x}_j) + \frac{\partial^2 \phi_i}{\partial y^2}(\mathbf{x}_j)\right) u_i^{(k)},$$

$$\nabla^2 v_j^{(k)} = \sum_{i=1}^{n} \left(\frac{\partial^2 \phi_i}{\partial x^2}(\mathbf{x}_j) + \frac{\partial^2 \phi_i}{\partial y^2}(\mathbf{x}_j) \right) v_i^{(k)}.$$

Also the homogenous Nuemann boundary conditions are enforced as

$$\sum_{i=1}^{n} \frac{\partial \phi_i}{\partial n}(\mathbf{x}_j) u_i^{(k+1)} = 0, \quad \mathbf{x}_j \in \partial\Omega, \tag{36}$$

and

$$\sum_{i=1}^{n} \frac{\partial \phi_i}{\partial n}(\mathbf{x}_j) v_i^{(k+1)} = 0, \quad \mathbf{x}_j \in \partial\Omega, \tag{37}$$

Thus Eqs. (34)-(37) constitute a $2n \times 2n$ system of nonlinear equations on the unknowns $u_i^{(k+1)}$ and $v_i^{(k+1)}$ for $i = 1, 2, \ldots, n$. Note we assume that $u_i^{(k)}$ and $v_i^{(k)}$ are known from the previous time level. At the first time level, i.e. when $k = 0$, $u_i^{(0)}$ and $v_i^{(0)}$ are computed using the initial conditions. At each time level a predicator-corrector scheme is used to solve the nonlinear equations, i.e. at first the system of linear equations

$$u_j^{(k+1)} - \beta \left(\nabla^2 u_j^{(k+1)} + \gamma \left(-u_j^{(k+1)} + u_j^{(k+1)} \tilde{u}_j \tilde{v}_j \right) \right) =$$
$$u_j^{(k)} + \beta \left(\nabla^2 u_j^{(k)} + \gamma \left(-u_j^{(k)} + (u_j^{(k)})^2 v_j^{(k)} \right) \right) + 2\beta\gamma a, \qquad \mathbf{x}_j \in \text{int}\,(\Omega), \tag{38}$$
$$v_j^{(k+1)} - \beta \left(d\nabla^2 v_j^{(k+1)} - \gamma v_j^{(k+1)} (\tilde{u}_j)^2 \right) =$$
$$v_j^{(k)} + \beta \left(d\nabla^2 v_j^{(k)} - \gamma (u_j^{(k)})^2 v_j^{(k)} \right) + 2\beta\gamma b, \qquad \mathbf{x}_j \in \text{int}\,(\Omega), \tag{39}$$

in which $\tilde{u}_j = u_j^{(k)}$ and $\tilde{v}_j = v_j^{(k)}$, is solved for unknowns $u_i^{(k+1)}$ and $v_i^{(k+1)}$ for $i = 1, 2, \ldots, n$, assuming that $u_i^{(k)}$ and $v_i^{(k)}$ are known from the previous time level. Then we put $\tilde{u}_j = u_j^{(k+1)}$ and $\tilde{v}_j = v_j^{(k+1)}$ in Eqs. (38) and (39) where $u_j^{(k+1)}$ and $v_j^{(k+1)}$ are just obtained and recompute $u_i^{(k+1)}$ and $v_i^{(k+1)}$ for $i = 1, 2, \ldots, n$. We iterate this procedure, until all the unknown quantities converge to within a prescribed number of significant figures. Once the prescribed convergence is achieved, we can move on to the following time level. The resulting solution from the current time level, provides the known values for the next time step. This process is repeated, until it approaches to the desirable time t. When $u(\mathbf{x}_j, t)$ and $v(\mathbf{x}_j, t)$, for all nodes $\{\mathbf{x}_j\}_{j=1}^{n}$, are obtained, the values of $u(\mathbf{x}, t)$ and $v(\mathbf{x}, t)$, at any point $\mathbf{x}$ in the domain problem Ω, are approximated using Eqs. (20) and (23), respectively as

$$u_h(\mathbf{x}, t) = \sum_{i=1}^{n} \phi_i(\mathbf{x}) u(\mathbf{x}_i, t), \quad v_h(\mathbf{x}, t) = \sum_{i=1}^{n} \phi_i(\mathbf{x}) v(\mathbf{x}_i, t), \qquad \mathbf{x} \in \bar{\Omega}. \tag{40}$$

A similar approach could be implemented to discretize other reaction–diffusion systems.

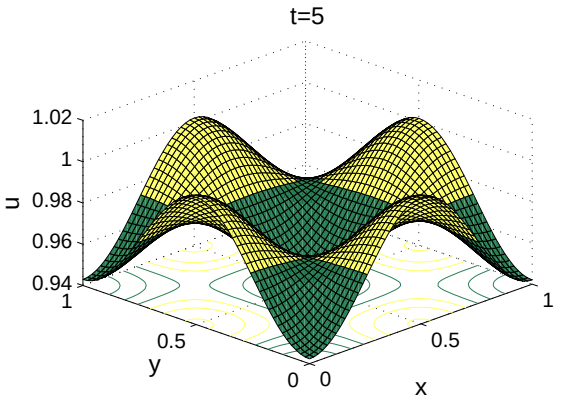

Figure 1: Numerical solution of the Schnakenberg model on the unit square with parameters $a = 0.1,\ b = 0.9,\ d = 8.6676$ and $\gamma = 230.82$. The solution surface of the activator u at $t = 5$, illustrating the type of shading used.

4 The numerical results

In this section, we have applied the finite point method to two reaction–diffusion systems. In all the cases we have used the quartic spline weight function:

$$w(r) = \begin{cases} 1 - 6r^2 + 8r^3 - 3r^4 & r \leq 1, \\ 0 & r > 1, \end{cases} \tag{41}$$

with $r = \frac{\|\mathbf{x}-\mathbf{x}_i\|}{d_i}$, where d_i is the support size of node i.

The number of boundary and interior nodes have stated in each case. Also in the proposed method, the second order approximation derivatives are needed. Thus, we have chosen $m = 6$ in computations.

In this paper, we plot the contour profiles of the solutions only. This is mainly for biological interpretation. In the biological context colour patterns are linked to cell differentiation. Assuming that coloration is determined by a constant threshold value in u (or v) concentration, u_s (or v_s) say, such that cells in the region where $u \geq u_s$ are yellow, while cells which experience a concentration $u < u_s$ are coloured green or blue, these give rise to the shading illustrated in all the figures. The actual solution surface u is as depicted in Fig. 1.

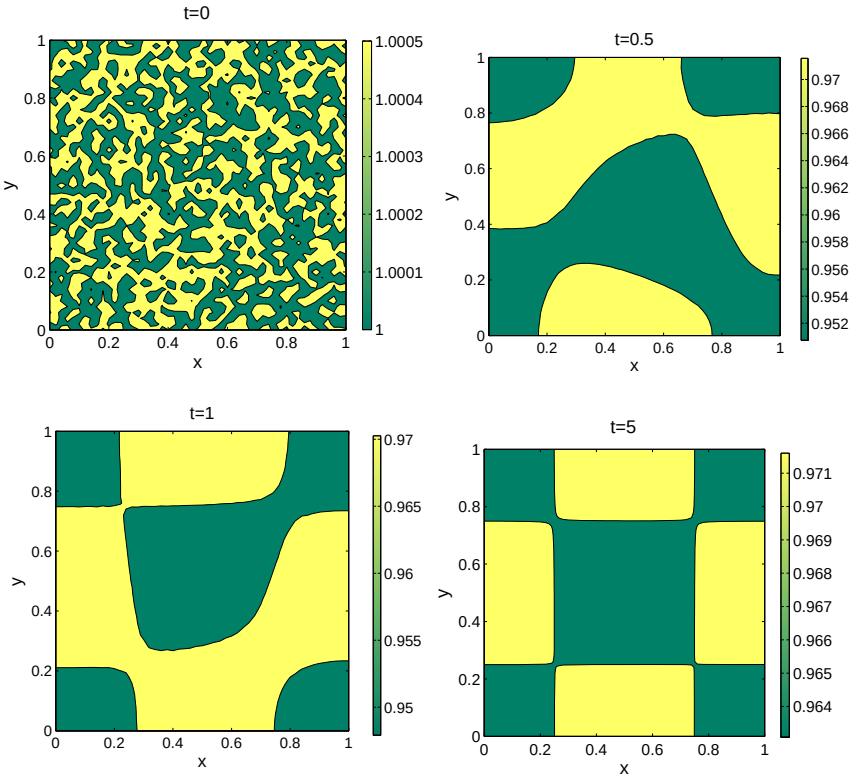

Figure 2: Numerical solution of the Schnakenberg model on the unit square with parameters $a = 0.1,\ b = 0.9,\ d = 8.6676$ and $\gamma = 230.82$. Contour plots of time evolution of the activator u at different times.

4.1 Schnakenberg model

4.1.1 Example 1

As a first numerical example consider the Schnakenberg model equations (4) and (5) on the unit square domain $\Omega = (0,1)^2$ with homogenous Neumann boundary conditions applied to both u and v. This system has a uniform positive steady state (u_s, v_s) given by $u_s = a + b$ and $v_s = b/(a+b)^2$. Let the parameter values $a = 0.1,\ b = 0.9,\ d = 8.6676$ and $\gamma = 230.82$. So $(u_s, v_s) = (1, 0.9)$ be the homogeneous steady state of this problem. Initial conditions are taken as small random perturbations around this steady state.

In computations we have used 2601 uniformly distributed collocation nodes in the

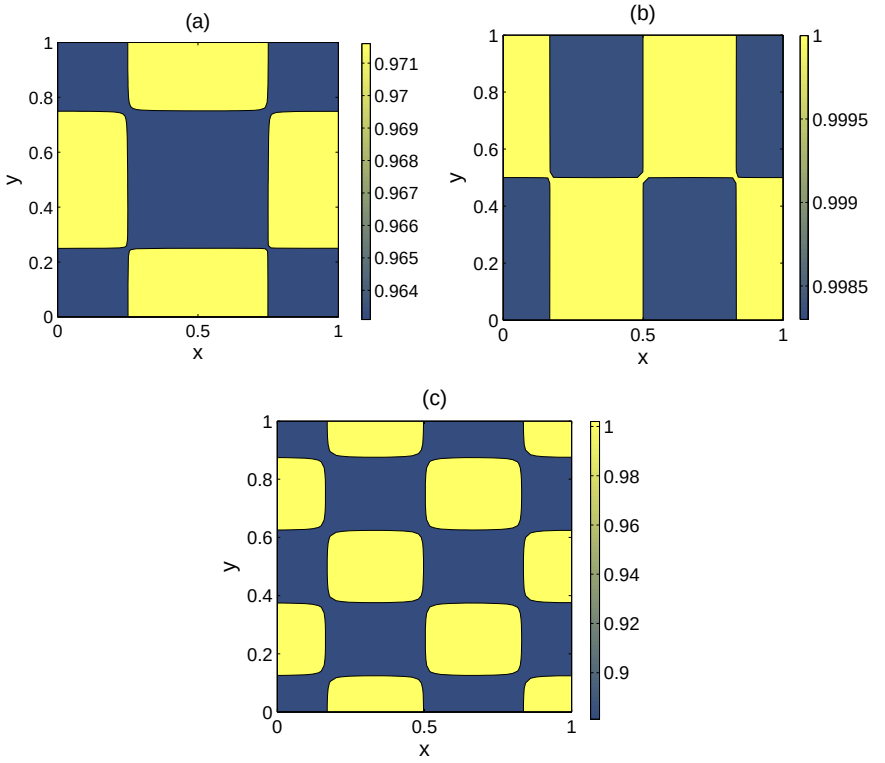

Figure 3: Contour plots of the activator u of the Schnakenberg model on the unit square with parameters $a = 0.1,\ b = 0.9,\ d = 8.6676$ and (a) $\gamma = 230.82$, (b) $\gamma = 329.20$ and (c) $\gamma = 666.82$.

domain problem $\Omega = (0,1)^2$ and on its boundary. The criterion for convergence to the inhomogeneous steady state is regarded as

$$E_u^{(k)} = \frac{\|\mathbf{u}^{(k+1)} - \mathbf{u}^{(k)}\|}{\|\mathbf{u}^{(k+1)}\|} < \varepsilon,$$

in which $\varepsilon = 10^{-7}$. In this case the inhomogeneous steady state is close to $T = 5$. To study the performance and convergence of the finite point method, we list in Tab. 2 the CPU time and error for simulations of the Schnakenberg model. The error at Δt is measured as a difference between this solution, $u_{\Delta t}$, and the solution $u_{2\Delta t}$ for time step size $2\Delta t$ at $T = 5$, i.e.,

$$E_{\Delta t} = \|u_{\Delta t} - u_{2\Delta t}\|. \tag{42}$$

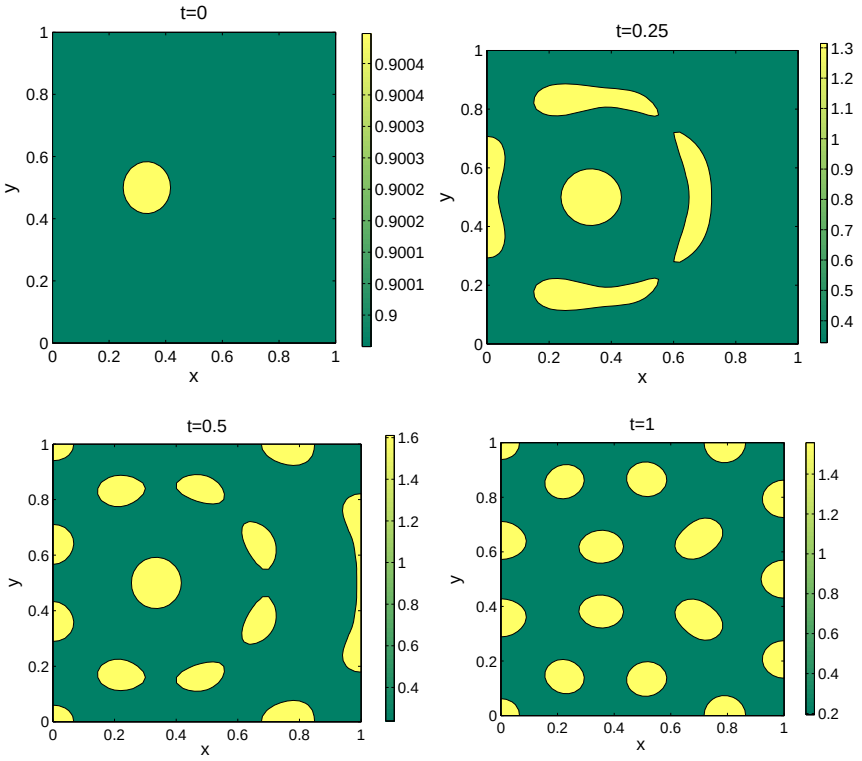

Figure 4: Numerical solution of the Schnakenberg model on the unit square with parameters $a = 0.1305,\ b = 0.7695,\ d = 20$ and $\gamma = 100$. Contour plots of time evolution of the activator u at different times.

The time evolution of the concentration of activator u is shown in Fig. 2. We can observe that the initial random perturbation is amplified and spreads, leading to formation of checkered pattern presented in Fig. 2. Moreover to study the effect of varying γ, we fix all parameter values $a,\ b,\ d$ and resolve the equation with $\gamma = 230.82$, $\gamma = 329.20$ and $\gamma = 666.82$. Fig. 3 shows the numerical simulations obtained by these values of γ.

4.1.2 Example 2

Consider the Schnakenberg model equations (4) and (5) with homogenous Neumann boundary conditions applied to both u and v as before. Following the setup

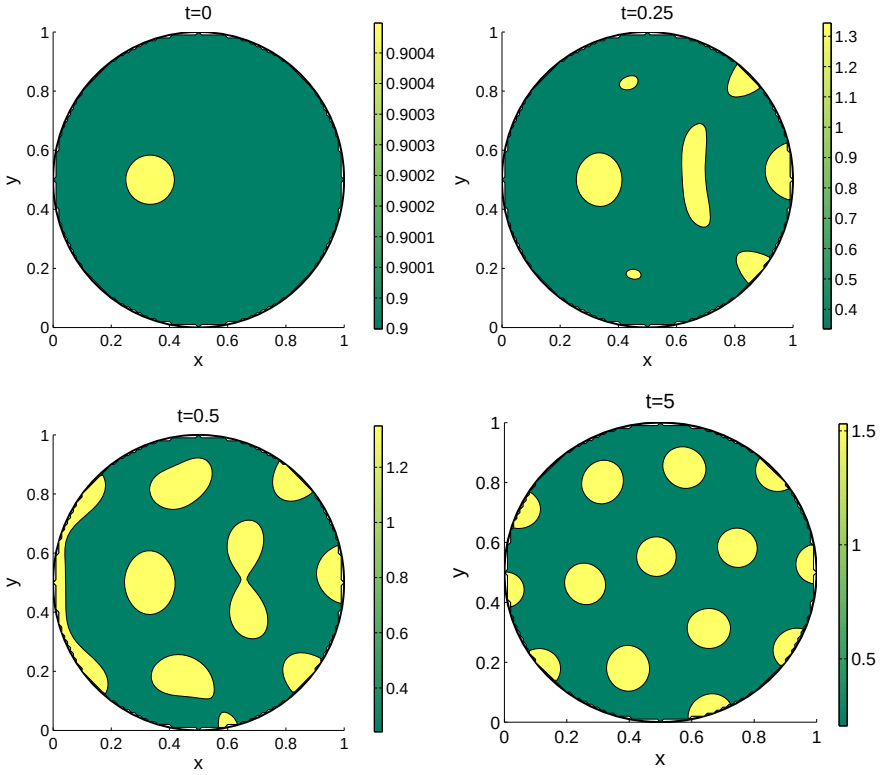

Figure 5: Numerical solution of the Schnakenberg model on a circular domain with parameters $a = 0.1305,\ b = 0.7695,\ d = 20$ and $\gamma = 100$. Contour plots of time evolution of the activator u at different times.

Table 2: CPU time and error for FPM applied to the Schnakenberg model in the unit square domain $(0,1)^2$, at T=5.

Δt	CPU time (s)	L^2 error	L^∞ error
1e-2	91	1.12 E-01	1.24 E-02
5e-3	150	1.84 E-02	1.32 E-03
1e-3	314	7.13 E-04	5.60 E-05
5e-4	895	5.94 E-05	4.67 E-06

in [Hundsdorfer and Verwer (2003)], we take the initial conditions as

$$u(x,y,0) = a+b+10^{-3}\exp\Big(-100((x-\frac{1}{3})^2+(y-\frac{1}{2})^2)\Big), \tag{43}$$

$$v(x,y,0) = \frac{b}{(a+b)^2}, \tag{44}$$

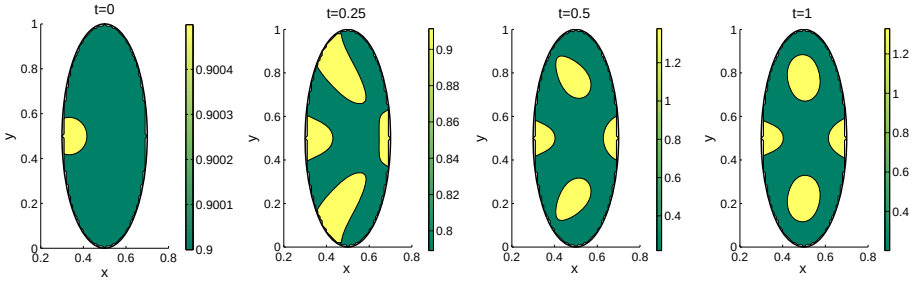

Figure 6: Numerical solution of the Schnakenberg model on an elliptical domain with parameters $a = 0.1305,\ b = 0.7695,\ d = 20$ and $\gamma = 100$. Contour plots of time evolution of the activator u at different times.

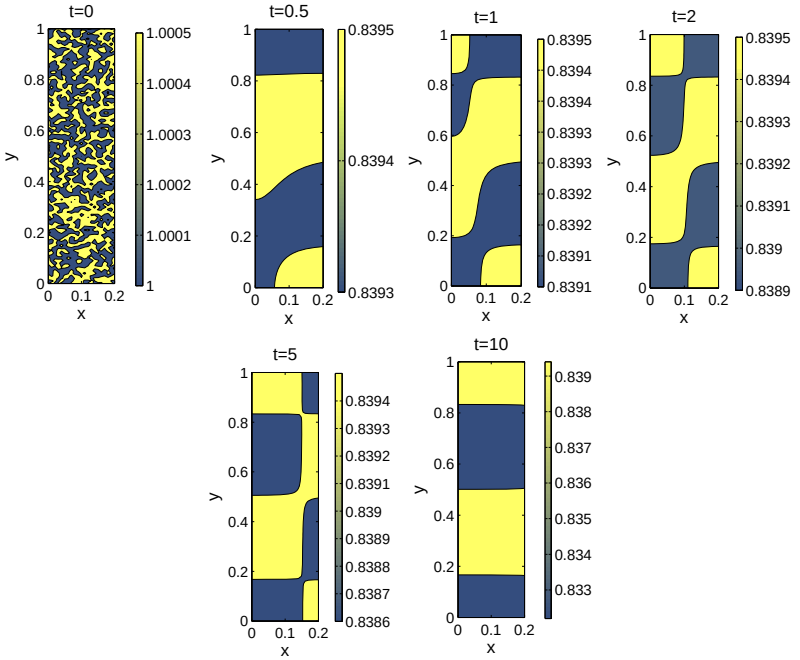

Figure 7: Numerical solution of the Gierer–Meinhardt model on a rectangular domain with parameters $a = 0.1,\ b = 1.0,\ K = 0.5,\ d = 70.8473$ and $\gamma = 619.45$. Contour plots of time evolution of the activator u at different times.

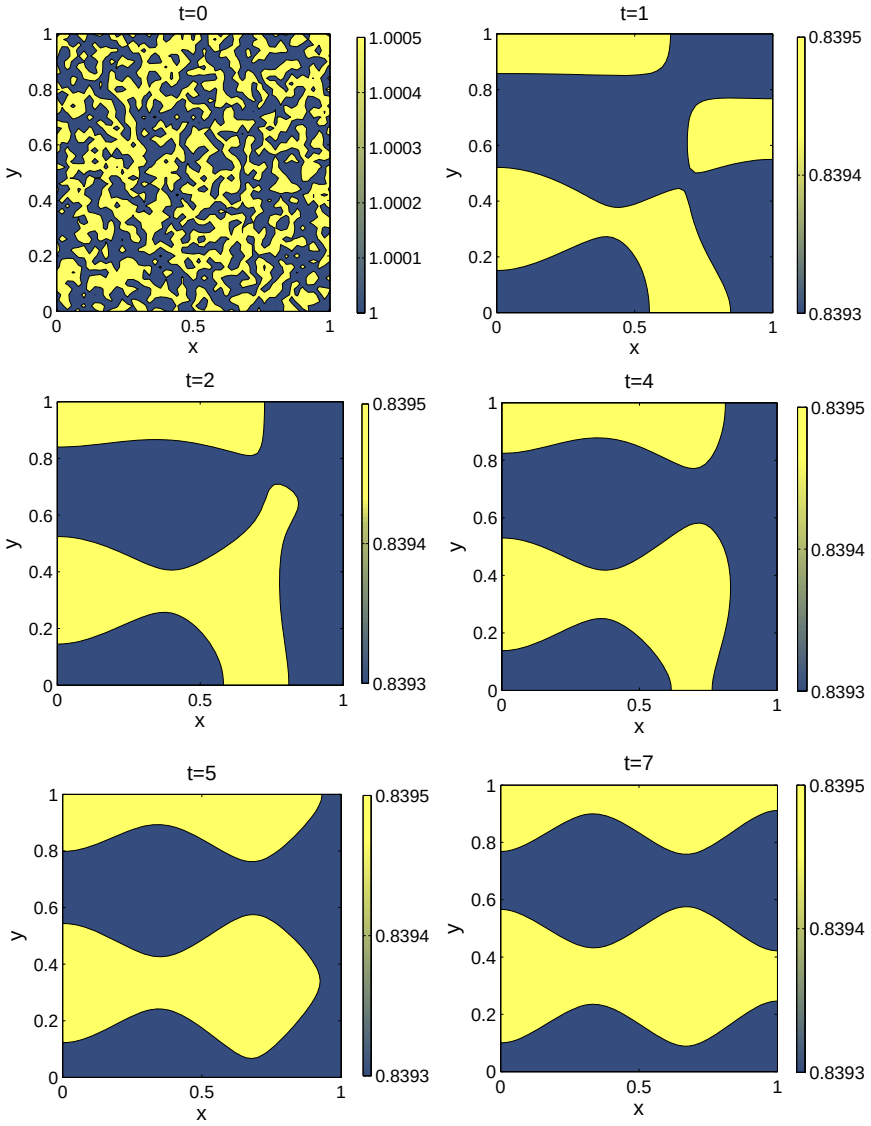

Figure 8: Numerical solution of the Gierer–Meinhardt model on a square domain with parameters $a = 0.1,\ b = 1.0,\ K = 0.5,\ d = 70.8473$ and $\gamma = 619.45$. Contour plots of time evolution of the activator u at different times.

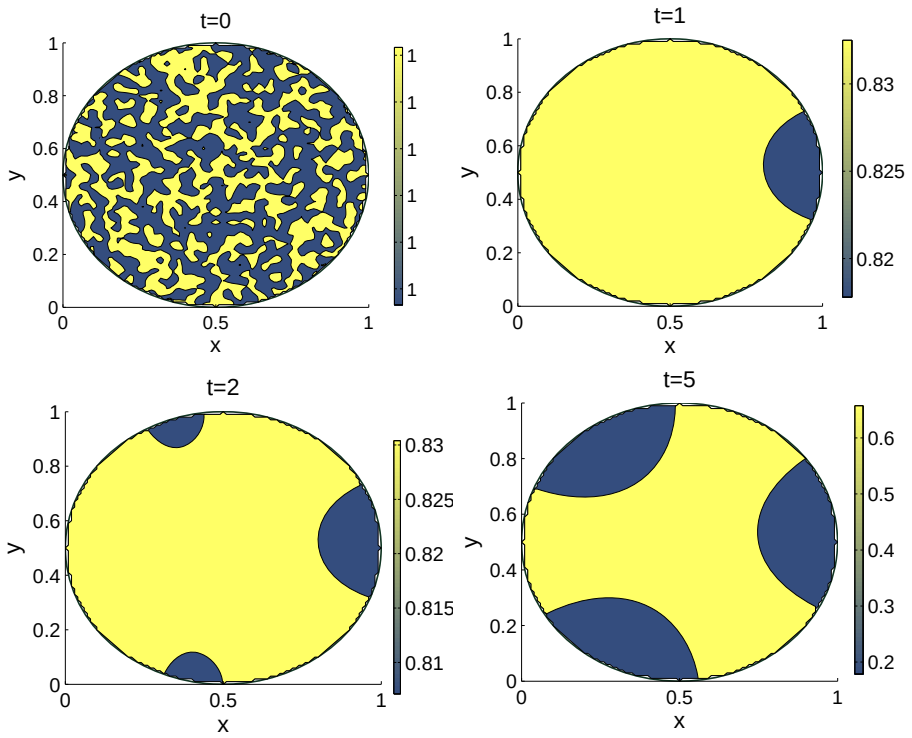

Figure 9: Numerical solution of the Gierer–Meinhardt model on a circular domain with parameters $a = 0.1,\ b = 1.0,\ K = 0.5,\ d = 70.8473$ and $\gamma = 619.45$. Contour plots of time evolution of the activator u at different times.

and the parameter values are $a = 0.1305,\ b = 0.7695,\ d = 20$ and $\gamma = 100$.

First we consider the equations on the unit square domain $\Omega = (0,1)^2$. The time evolution of the activator u obtained by 2601 collocation nodes is shown in Fig. 4. We can observe that the initial perturbation in (43) and (44) is amplified and spreads, leading to formation of spot–like patterns.

Next we vary the shape and size of the domain, but keep all of parameters unchanged. The time evolution plots of concentrations of activator u are shown in Fig. 5 for the circular domain $\Omega = \left\{(x,y)|(x-0.5)^2+(y-0.5)^2 < 0.5^2\right\}$ and Fig. 6 for the elliptic domain $\Omega = \left\{(x,y)|(\frac{x-0.5}{0.25})^2+(\frac{y-0.5}{0.5})^2 < 1\right\}$. In computations we have used 2092+151 collocation nodes in the circular domain and on its boundary and 919+151 collocation nodes in the elliptic domain.

It is interesting to notice that spot–like patterns are formed on the circular and elliptic domains (Figs. 5 and 6) like the square domain.

Also we list in Tab. 3 the CPU time and error for simulations of the Schnakenberg model on the circular domain at $T = 5$, close to steady state.

Table 3: CPU time and error for FPM applied to the Schnakenberg model in the circular domain, at T=5.

Δt	CPU time (s)	L^2 error	L^∞ error
1e-2	286	8.92 E-02	3.17 E-02
5e-3	571	7.23E-03	1.85E-03
1e-3	1125	9.41E-05	5.81E-05
5e-4	1937	1.06E-05	2.13E-06

4.2 Gierer–Meinhardt model

4.2.1 Example 3

In this example we solve the Gierer–Meinhardt reaction kinetics with homogenous Neumann boundary conditions for both u and v. Initial conditions are taken as random perturbations about a constant value. We fix the parameter values $a = 0.1,\ b = 1.0,\ K = 0.5,\ d = 70.8473,\ \gamma = 619.45$ and only vary the shape of the domain.

The time evolution plots of activator u are shown in Fig. 7 for a rectangular domain with 561 collocation nodes, Fig. 8 for a square domain with 2601 collocation nodes and Fig. 9 for a circular domain with 151+2092 collocation nodes. We observe the transition of stripe patterns to spot patterns on the narrow rectangular domain to the circular domain. These simulations of the Gierer–Meinhardt system on different domains provide an example of the sensitivity of patterns in reaction–diffusion systems with respect to the domain size and shape.

Also the CPU time and error for simulations of the Gierer–Meinhardt model have been shown in Tab. 4 on the unit square at $T = 7$ and Tab. 5 on the circular domain at $T = 5$.

5 Conclusion

In this paper the numerical solution of the reaction–diffusion system has been studied using the finite point method. The numerical solutions for two cases, the Schnakenberg model and the Gierer–Meinhardt model have been presented in various regions to demonstrate the effects of various domain geometries on the resulting

Table 4: CPU time and error for FPM applied to the Gierer–Meinhardt model in the unit square, at T=7.

Δt	CPU time (s)	L^2 error	L^∞ error
2e-3	972	9.12 E-03	8.27 E-03
1e-3	1674	3.61 E-04	1.35 E-04
5e-4	2851	7.42 E-06	2.51 E-06
2.5e-4	4312	3.73 E-06	8.13E-07

Table 5: CPU time and error for FPM applied to the Gierer–Meinhardt model in the circular domain, at T=5.

Δt	CPU time (s)	L^2 error	L^∞ error
2e-3	841	7.42 E-03	4.31 E-03
1e-3	1138	5.31 E-04	2.75 E-04
5e-3	2231	3.12 E-06	1.23 E-06
2.5e-4	3986	2.75 E-07	1.34 E-07

biological patterns. The method is a truly meshfree method, which requires neither domain elements nor integrations and our numerical examples show good results, with the accuracy of solving the reaction–diffusion systems. The simplicity in the implementation shows the efficiency of the finite point method.

However the focus in this paper is on the FPM for solving the reaction–diffusion systems in fix domains but this method could be implemented for reaction–diffusion problems in growing domains.

References

Atluri, S. N. (2005): *The meshless method (MLPG) for domain and BIE discretizations*. Tech. Science Press.

Atluri, S. N.; Shen, S. (2002): *The Meshless Local Petrov–Galerkin (MLPG) Method*. Tech. Science Press.

Atluri, S. N.; Shen, S. (2002): The meshless local Petrov–Galerkin (MLPG) method: a simple and lesscostly alternative to the finite element and boundary element methods. *CMES: Computer Modeling in Engineering & Sciences*, vol. 3, pp. 11–52.

Atluri, S. N.; Zhu, T. (1998): A new meshless local Petrov–Galerkin (MLPG) approach in computational mechanics. *Comput. Mech.*, vol. 22, pp. 117–127.

Barrio, S. R.; Varea, C.; Aragn, J.; Maini, P. (1999): A two-dimensional numerical study of spatial pattern formation in interacting systems. *Bull. Math. Biol.*, vol. 61, pp. 483–505.

Baurmanna, M.; Gross, T.; Feudel, U. (2007): Instabilities in spatially extended predator–prey systems: spatio–temporal patterns in the neighborhood of Turing–Hopf bifurcations. *J. Theor. Biol.*, vol. 245, pp. 220–229.

Belytschko, T.; Lu, Y.; Gu, L. (1994): Element free Galerkin methods. *Int. J. Num. Meth. Eng.*, vol. 37, pp. 229–256.

Boroomand, B.; Najjar, M.; Onate, E. (2009): The generalized finite point method. *Computational Mechanics*, vol. 44, pp. 173–190.

Chaplain, M.; Ganesh, A.; Graham, I. (2001): Spatio–temporal pattern formation on spherical surfaces: numerical simulation and application to solid tumor growth. *J. Math. Biol.*, vol. 42, pp. 387–423.

Crampin, E.; Gaffney, E.; Maini, P. (1999): Reaction and diffusion on growing domains: Scenarios for robust pattern formation. *J. Math. Biol.*, vol. 61, pp. 1093–1120.

Dehghan, M.; Ghesmati, A. (2010): Combination of meshless local weak and strong (MLWS) forms to solve the two dimensional hyperbolic telegraph equation. *Analysis with Boundary Elements*, vol. 34, pp. 324–336.

Dehghan, M.; Mirzaei, D. (2009): Meshless local Petrov–Galerkin (MLPG) method for the unsteady magnetohydrodynamic (MHD) flow through pipe with arbitrary wall conductivity. *Applied Numerical Mathematics*, vol. 59, pp. 1043–1058.

Dehghan, M.; Salehi, R. (2011): A boundaryonly meshless method for numerical solution of the Eikonal equation. *Computational Mechanics*, vol. 47, pp. 283–294.

Dehghan, M.; Salehi, R. (2011): The solitary wave solution of the two–dimensional regularized long wave equation in fluids and plasmas. *Computer Physics Communications*, vol. 182, pp. 2540–2549.

Dehghan, M.; Shokri, A. (2008): A numerical method for solution of the two–dimensional Sine–Gordon equation using the radial basis functions. *Mathematics and Computers in Simulation*, vol. 79, pp. 700–715.

Dolbow, J.; Belytschko, T. (1998): An introduction to programming the meshless element free Galerkin method. *Comput. Meth. Eng.*, vol. 5, no. 3, pp. 207–241.

Ferreira, S.; Martins, M.; Vilela, M. (2002): Reaction–diffusion model for the growth of avascular tumor. *Phys. Rev.*, vol. 65, no. 2, pp. 1467–1476.

Frederik, H.; Maini, P.; Madzvamuse, A.; Wathen, A.; Sekimura, T. (2003): Pigmentation pattern formation in butterflies: experiments and models. *C. R. Biol.*, vol. 326, pp. 717–727.

García-Aznar, J.; Kuiper, J.; Gómez-Benito, M.; Doblaré, M.; Richardson, J. (2007): Computational simulation of fracture healing: influence of interfragmentary movement on the callus growth. *J. Biomech.*, vol. 40, pp. 1467–1476.

Garzón-Alvarado, D.; Galeano, C.; Mantilla, J. (2011): Turing pattern formation for reaction–convection–diffusion systems in fixed domains submitted to toroidal velocity fields. *Applied Mathematical Modelling*, vol. 35, pp. 4913–4925.

Gierer, A.; Meinhardt, H. (1972): A theory of biological pattern formation. *kybernetic*, vol. 12, pp. 30–39.

Hundsdorfer, W.; Verwer, J. (2003): *Numerical solution of time–dependent advection–diffusion–reaction equations*. Springer.

Kassam, A.; Trefethen, L. (2003): Solving reaction–diffusion equations 10 times faster. *Oxford University: Numerical Analysis Group Research, Report 16*.

Kim, D. W.; Liu, W. K. (2006): Maximum principle and convergence analysis for the meshfree point collocation method. *SIAM J. Numer. Anal.*, vol. 44, no. 2, pp. 515–539.

Kim, D. W.; Liu, W. K.; Yoon, Y.-C.; Belytschko, T.; Lee, S.-H. (2007): Meshfree point collocation method with intrinsic enrichment for interface problems. *Comput. Mech.*, vol. 40, pp. 1037–1052.

Kim, D. W.; Yoon, Y.-C.; Liu, W. K.; Belytschko, T. (2007): Extrinsic meshfree approximation using asymptotic expansion for interfacial discontinuity of derivative. *J. Comput. Phys.*, vol. 221, pp. 370–394.

Kondo, S.; Asai, R. (1995): A reaction–diffusion wave on the skin of the marine anglefish Pomacanthus. *Nature*, vol. 376, pp. 765–768.

Li, S.; Liu, W. K. (2004): *Meshfree particle methods*. Springer.

Liszka, T.; Orkisz, J. (1975): The finite difference method at arbitrary irregular grids and its application in applied mechanics. *Comp. Struct.*, vol. 11, pp. 38–95.

Liu, W.; Chen, Y.; Jun, S.; Chen, J.; Belytschko, T.; Pan, C.; Uras, R.; Chang, C. (1996): Overview and applications of the reproducing kernel particle method. *Archives of Comput. Meth. Eng.*, vol. 3, no. 1, pp. 3–80.

Liu, W.; Jun, S.; Li, S.; Adee, J.; Belytschko, T. (1995): Reproducing kernel particle methods for structural dynamics. *Int. J. Num. Meth. Eng.*, vol. 5, no. 3, pp. 1655–1679.

Liu, W.; Jun, S.; Zhang, Y. (1995): Reproducing kernel particle method. *Int. J. Numer. Meth. Fluids*, vol. 20, pp. 1081–1106.

Liu, W. K.; Li, S.; Belytschko, T. (1997): Moving least squares reproducing kernel methods, Part I: Methodology and convergence. *Comput. Methods Appl. Mech. Engrg.*, vol. 143, pp. 113–154.

Madzvamuse, A. (2000): *A Numerical Approach to the Study of Spatial Pattern Formation*. Ph.D. Thesis, University of Oxford.

Madzvamuse, A.; Maini, P. (2007): Velocity-induced numerical solution of reaction-diffusion systems on continuously growing domains. *Journal of Computational Physics*, vol. 225, pp. 100–119.

Madzvamuse, A.; Thomas, R.; Maini, P.; Wathen, A. (2002): A numerical approach to the study of spatial pattern formation in the ligaments of arcoid bivalves. *Bull. Math. Biol.*, vol. 64, pp. 501–530.

Madzvamuse, A.; Wathen, A.; Maini, P. (2003): A moving grid finite element method applied to a model biological pattern generator. *Journal of Computational Physics*, vol. 190, pp. 478–500.

Madzvamuse, A.; Wathen, A.; Maini, P. (2005): A moving grid finite element method for the simulation of pattern generation by Turing models on growing domains. *J. Sci. Comput.*, vol. 24, pp. 247–262.

Meinhardt, H. (1982): *Models of Biological Pattern Formation*. Academic Press, New York.

Mirzaei, D.; Dehghan, M. (2010): A meshless based method for solution of integral equations. *Applied Numerical Mathematics*, vol. 60, pp. 245–262.

Monaghan, J. (1992): Smoothed particle hydrodynamics: Some recent improvement and applications. *Annu. Rev. Astron. Physics*, vol. 30, pp. 543–574.

Murray, J. (1981): A prepattern formation mechanism for animal coat markings. *J. Theor. Biol.*, vol. 88, pp. 161–199.

Murray, J. (1993): *Mathematical Biology*. Springer.

Nayroles, B.; Touzot, G.; Villon, P. (1992): Generalizing the FEM: Diffuse approximation and diffuse elements. *Comput. Mechanics*, vol. 10, pp. 307–318.

Onate, E.; Idelsohn, S. (1998): A meshfree finite point method for advective–diffusive transport and fluid flow problems. *Computational Mechanics*, vol. 21, pp. 283–292.

Onate, E.; Idelsohn, S.; Zienkiewicz, O.; Fisher, T. (1995): Finite point method for analysis of fluid flow problems. *Proceedings of the 9th Int. Conference on Finite Element Methods in Fluids. Venize, Italy*, pp. 15–21.

Onate, E.; Idelsohn, S.; Zienkiewicz, O.; Taylor, R. (1996): A finite point method in computational mechanics, Applications to convective transport and fluid flow. *Int. J. Num. Meth. Eng.*, vol. 39, pp. 3839–3866.

Onate, E.; Idelsohn, S.; Zienkiewicz, O.; Taylor, R. (1996): A stabilized finite point method for analysis of fluid mechanics's problems. *Comput. Meth. Appl. Eng.*, vol. 139, pp. 315–347.

Perrone, N.; Kao, R. (1975): A generalized finite difference method for arbitrary meshes. *Comp. Struct.*, vol. 5, pp. 45–47.

Randles, P.; Libersky, L. (1996): Smoothed particle hydrodynamics: Some recent improvement and applications. *Comp. Meth. Appl. Mech. Eng.*, vol. 139, pp. 375–408.

Rossi, F.; Ristori, S.; Rustici, M.; Marchettini, N.; Tiezzi, E. (2008): Dynamics of pattern formation in biomimetic systems. *J. Theor. Biol.*, vol. 255, pp. 404–412.

Schnakenberg, J. (1979): Simple chemical reaction systems with limit cycle behavior. *J. Theoret. Biol.*, vol. 81, pp. 389–400.

Sekimura, T.; Madzvamuse, A.; Wathen, A.; Maini, P. (2000): A model for colour pattern formation in the butterfly wing of Papilio dardanus. *Proc. Roy. Soc. Lond. Ser. B*, vol. 26, pp. 852–859.

Shakeri, F.; Dehghan, M. (2011): The finite volume spectral element method to solve Turing models in the biological pattern formation. *Computers and mathematics with applications*, vol. 62, pp. 4322–4336.

Shokri, A.; Dehghan, M. (2010): A meshless method the using radial basis functions for numerical solution of the regularized long wave equation. *Numer. Methods Partial Differential Eq.*, vol. 26, pp. 807–825.

Sladek, J.; Sladek, V.; Atluri, S. N. (2004): Meshless local Petrov-Galerkin method for heat conduction problem in an anisotropic medium. *CMES: Computer Modeling in Engineering and Sciences*, vol. 6, pp. 309–318.

Sladek, J.; Sladek, V.; Hellmich, C.; Eberhardsteiner, J. (2007): Heat conduction analysis of 3D axisymmetric and anisotropic FGM bodies by meshless local Petrov-Galerkin method. *Computational Mechanics*, vol. 39, pp. 223–233.

Sladek, J.; Sladek, V.; J. Krivacek, C. Z. (2003): Local BIEM for transient heat conduction analysis in 3-D axisymmetric functionally graded solids. *Computational Mechanics*, vol. 32, pp. 169–176.

Sladek, J.; Sladek, V.; Tan, C.; Atluri, S. N. (2008): Analysis of transient heat conduction in 3D anisotropic functionally graded solids, by the MLPG method. *CMES: Computer Modeling in Engineering and Sciences*, vol. 32, pp. 161–174.

Sladek, J.; Sladek, V.; Zhang, C. (2004): A local BIEM for analysis of transient heat conduction with nonlinear source terms in FGMs. *Engineering Analysis with Boundary Elements*, vol. 28, pp. 1–11.

Tatari, M.; Dehghan, M. (2009): On the solution of the non–local parabolic partial differential equations via radial basis functions. *Applied Mathematical Modelling*, vol. 33, pp. 1729–1738.

Tatari, M.; Kamranian, M.; Dehghan, M. (2011): The finite point method for the *p*–Laplace equation. *Computational Mechanics, DOI 10.1007/s00466-011-0613-6*.

Thomas, D.; Kervenez, J.-P. (1975): *Analysis and Control of Immobilised Enzyme Systems*. Springer.

Turing, A. (1952): The chemical basis of morphogenesis. *Philos. Trans. Roy. Soc. Lond.*, vol. 237, pp. 37–72.

Yi, F.; Wei, J.; Shi, J. (2009): Bifurcation and spatiotemporal patterns in a homogeneous diffusive predator–prey system . vol. 246, no. 5, pp. 1944–1977.

Zhu, T.; Zhang, J.; Atluri, S. N. (1998): A local boundary integral equation (LBIE) method in computational mechanics, and a meshless discretization approach. *Computational Mechanics*, vol. 21, pp. 223–235.

Zuppa, C. (2003): Error estimates for moving least squares approximations. *Bull. Brazil Math. Soc.*, vol. 34, no. 2, pp. 231–249.